ELSEVIER

Contents lists available at ScienceDirect

Science Bulletin

journal homepage: www.elsevier.com/locate/scib



Article

Functionalization of small black phosphorus nanoparticles for targeted imaging and photothermal therapy of cancer

Lijuan Deng ^{a,b}, Yifan Xu ^{a,b}, Caixia Sun ^b, Baofeng Yun ^c, Qiao Sun ^b, Chongjun Zhao ^{a,*}, Zhen Li ^{b,*}

ARTICLE INFO

Article history: Received 20 March 2018 Received in revised form 19 April 2018 Accepted 2 May 2018 Available online 25 May 2018

Keywords:
Black phosphorus
Functionalization
Targeted imaging
Photothermal therapy

ABSTRACT

Black phosphorus (BP) nanomaterials have attracted extensive attention due to their unique physical, chemical, and biological properties. In this study, small BP nanoparticles were synthesized and modified with dextran and poly(ethyleneimine) for functionalization with folic acid and cyanine 7. The functionalized BP nanoparticles exhibit excellent biocompatibility, stability, and near infrared optical properties for targeted imaging of tumors through photoacoustic imaging and near-infrared fluorescence imaging. They also display high photothermal conversion efficiency for photothermal therapy of cancer. This work demonstrates the potential of functionalized small BP nanoparticles as an emerging nanotheranostic agent for the diagnosis and treatment of cancer.

© 2018 Science China Press. Published by Elsevier B.V. and Science China Press. All rights reserved.

1. Introduction

Black phosphorus (BP) is similar to other two-dimensional (2D) nanomaterials [1,2], has attracted extensive attention due to its unique physical, chemical, and biological properties. BP was first synthesized in 1914 [3]. BP is the most stable one among the three allotropes of phosphorus [4]. Semiconductive BP has a tunable band gap from 0.3 to 2.0 eV, which is dependent on the thickness (layers) of BP [5,6]. In addition, BP also has unique mechanical, electrical, and thermal anisotropy for various promising applications, including transistors [7,8], memory devices [9], photodetectors [10,11], energy storage [12,13], gas sensors [14,15], etc.

It is well known that phosphorus is an essential element in humans, and BP has an excellent photothermal effect under near-infrared (NIR) irradiation, which gives it great potential in biomedical fields. For example, BP nanodots have been used for fluorescence bioimaging [16], photoacoustic (PA) imaging [17,18], and photothermal therapy (PTT) [19]. BP nanosheets could be used as a photosensitizer for photodynamic therapy (PDT) [20]. To improve their efficacy in diagnosis and treatment, surface functionalization of BP nanomaterials has become an important

 $\it E-mail\ addresses:\ chongjunzhao@ecust.edu.cn\ (C.\ Zhao),\ zhenli@suda.edu.cn\ (Z.\ Li).$

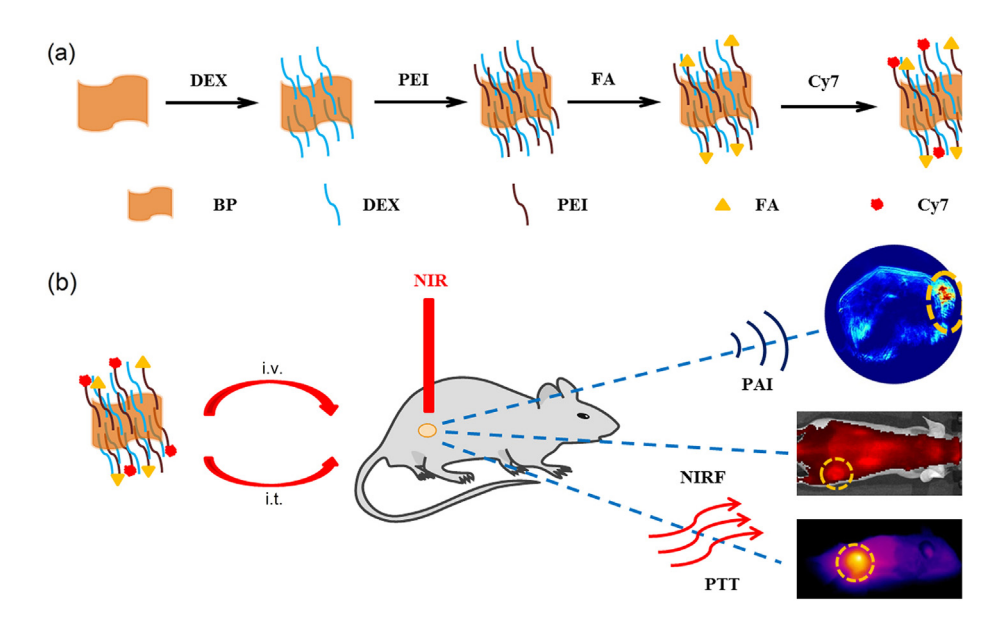
strategy. For example, BP nanosheets were modified with poly (ethylene glycol)-amine (PEG-NH₂) to overcome the adsorption of proteins [21], and were loaded with iron oxide (Fe₃O₄) and Au nanoparticles to introduce more functions for cancer theranostics [22]. However, most modification and functionalization are performed on large BP nanosheets. There are few reports on the functionalization of small BP nanoparticles. Compared with large BP nanosheets, small nanoparticles exhibit long blood circulation and fast clearance and degradation [23,24].

In this article, water-soluble and biocompatible small BP nanoparticles were prepared by a simple one-pot solventless high energy mechanical milling (HEMM) approach [17]. As illustrated in Scheme 1a, BP nanoparticles were modified in situ with dextran (DEX) and branched poly(ethyleneimine) (PEI) during ball milling to endow them with biocompatibility, solubility, stability, and functional groups (i.e., -NH₂). The BP-DEX/PEI nanoparticles were then conjugated with folic acid (FA) to improve their accumulation in tumors for targeted PA imaging, and also conjugated with the fluorescent dye sulfocyanine7 N-hydroxysuccinimide (NHS) ester (Cy7-SE) for complementary near-infrared fluorescence (NIRF) imaging [25]. The functionalized BP nanoparticles also show high photothermal conversion efficiency for PTT of cancer. Our work illustrates the potential of multifunctional BP nanotheranostics for dual-modal imaging-guided PTT of cancer [26-30].

^a Key Laboratory for Ultrafine Materials of Ministry of Education, Shanghai Key Laboratory of Advanced Polymeric Materials, School of Material Science and Engineering, East China University of Science and Technology, Shanghai 200237, China

b Center for Molecular Imaging and Nuclear Medicine, State Key Laboratory of Radiation Medicine and Protection, School for Radiological and Interdisciplinary Sciences (RAD-X), Collaborative Innovation Center of Radiation Medicine of Jiangsu Higher Education Institutions, Soochow University, Suzhou 215123, China College of Textile and Clothing Engineering, Soochow University, Suzhou 215123, China

^{*} Corresponding authors.



Scheme 1. (Color online) Schematic illustration of the synthesis of surface functionalized BP (BP-DEX/PEI-FA/Cy7) nanoparticles (a) and their applications (b) in PA imaging, NIRF imaging, and photothermal therapy of cancer (i.t.: intratumoral injection, i.v.: intravenous injection).

2. Experimental

2.1. Materials

Red phosphorus (RP) was purchased from Sinopharm Chemical Reagent Co., Ltd. DEX ($M_{\rm w}$ = 20,000), PEI ($M_{\rm w}$ = 1800) and N-(3-dimethylaminopropyl)-N-ethylcarbodiimide hydrochloride (EDC, 98.5%) were all obtained from Aladdin. FA (97%) was provided by Shanghai Qiangshun Chemical Reagent Co., Ltd. N-hydroxysuccinimide (NHS, 98%) was purchased from J&K Chemical Ltd. Cy7-SE (95%) was purchased from Okeanos.

2.2. Synthesis of BP-DEX/PEI nanoparticles

BP nanoparticles were synthesized using the ball-milling approach [17]. Firstly, 500 mg BP and 2 g DEX were added into a ball-milling jar, and the mixture was milled for 12 h to produce BP-DEX powder. Secondly, 1 g BP-DEX powder was mixed with 50 mg PEI and milled for another 12 h. Then, the powder was dispersed in 100 mL $\rm H_2O$. The resultant dispersion was centrifuged at a speed of 10,000 r/min for 20 min. The supernatant was further purified by ultrafiltration at 4000 r/min by using a membrane with a molecular weight cut-off of 100 kDa to yield a BP-DEX/PEI solution, which was stored at 4 °C for further use.

2.3. Functionalization of BP-DEX/PEI nanoparticles

A 10.2 mg FA, 21.8 mg EDC, and 14.1 mg NHS were added into 20 mL of phosphate buffered saline (PBS, pH 7.4) in a sequential order, and the mixture was stirred at room temperature in the dark for 4 h. BP-DEX/PEI (5 mg/mL, 4 mL) aqueous solution was then added into the above reaction mixture under continuous stirring at room temperature for overnight in the dark. After the reaction, excess FA in the as-synthesized BP-DEX/PEI-FA sample was removed by ultrafiltration through Amicon centrifugal filters with 100 kDa molecular weight cut-off (MWCO) and washed with PBS 8 times

The purified BP-DEX/PEI-FA ($200~\mu g/mL$) was reacted with Cy7-SE ($100~\mu g/mL$) in PBS solution with a pH of 7.4. The reaction was allowed to proceed overnight in the dark at room temperature. Excess dye molecules were removed by ultrafiltration through

100 kDa MWCO Amicon filters and washed with water for more than 10 times until no Cy7 was detected in the filtrate solution. Then, the BP-DEX/PEI-FA/Cy7 solution was stored at $4\,^{\circ}$ C.

2.4. Characterization of BP nanoparticles

The morphology of the BP nanoparticles was characterized with a FEI Tecnai F20 transmission electron microscope (TEM) operating at 200 kV. The hydrodynamic size was measured at 25 °C with a Malvern Zetasizer Nano ZS90. Ultraviolet–visible-near-infrared (UV–Vis-NIR) spectra were recorded with a PerkinElmer Lambda 750 UV–Vis-NIR spectrophotometer. Fourier transform infrared (FTIR) spectra were recorded on a Magna-560 spectrometer. X-ray photoelectron spectroscopy (XPS) measurements were recorded using a Thermo Scientific Sigma Probe instrument with Al K α X-ray radiation and fixed analyzer transmission mode. The crystal structure of the nanoparticles was characterized by X-ray diffraction (XRD) with a Shimadzu XRD-600 with Cu K α 1 radiation (λ = 0.15405 nm).

2.5. Cytotoxicity assay of BP nanoparticles

Murine breast cancer cells (4T1) and mouse embryo fibroblasts cells (3T3) (1 \times 10^4 cells/well) were seeded into 96-well plates in standard cell media, cultured at 37 °C in a 5% CO2 atmosphere, and then incubated with BP-DEX/PEI and BP-DEX/PEI-FA nanoparticles at different concentrations (i.e., 3.125, 6.25, 12.5, 25, 50, and 100 $\mu g/mL)$ for 12 h. The relative cell viabilities were determined by the standard 3-(4,5-dimethylthiazol-2-yl)-2, 5-diphenyltetrazolium bromide (MTT) assay.

2.6. Tumor model

The 4T1 tumor models were generated by subcutaneous injection of 2×10^6 cells in 50 μL of PBS into the flank region of the right backs of 5-week-old male BALB/c mice (for the PTT treatment) or nude mice (for the PA imaging and NIRF imaging). The tumor imaging studies were carried out at 8 d after the inoculation with tumor cells. All animal experiments were carried out according to the protocols approved by the Soochow University Laboratory Animal Center.

2.7. Photoacoustic (PA) imaging

In vitro PA imaging was performed on a multispectral optoacoustic tomography scanner (MSOT, iThera Medical). A series of BP-DEX/PEI-FA nanoparticle solutions (0, 12.5, 25, 50, 100, and 200 μ g/mL) were prepared for in vitro test. For in vivo PA imaging, nude mice bearing subcutaneous tumors were anesthetized with 1.5% isoflurane delivered via a nose cone, and then BP-DEX/PEI and BP-DEX/PEI-FA nanoparticles (2 mg/mL of P, 200 μ L) were injected via the tail vein. PA images were acquired at different time points post injection by a multispectral optoacoustic tomography instrument. Ten slices were obtained at each position and averaged to minimize the influence of animal movement on the images.

2.8. NIRF imaging

For in vivo NIRF imaging, BP-DEX/PEI-Cy7 and BP-DEX/PEI-FA/Cy7 nanoparticles (2 mg/mL of P, 200 $\mu L)$ were injected via the tail vein into the mice bearing 4T1 tumors. Then, under isoflurane anesthesia, the in vivo NIRF imaging was performed using an IVIS Lumina II imaging system at different time points' post injection, respectively. The excitation wavelength for the NIRF imaging is 750 nm.

2.9. In vivo photothermal therapy

BP-DEX/PEI-FA/Cy7 (50 μ L, 2 mg/mL) or PBS solution was intratumorally injected into tumor-bearing mice, which were irradiated for 6 min with an 808 nm NIR laser at a power density of 1.5 W/cm². The tumor sizes and body weights were measured every 2 days, and the tumor volume was expressed by $L \times W^2/2$, where L and W represent the length and width of the tumor, respectively.

2.10. Histological analysis

The mice from the control group or treatment group were sacrificed to resect their heart, liver, spleen, lung, and kidney. The major organs were dipped in 10% formalin, processed routinely into paraffin, sectioned into thin slices, and stained with hematoxylin and eosin stain (H&E) for histological analysis.

3. Results and discussion

3.1. Characterization of BP-DEX/PEI nanoparticles

The morphology and size of the as-prepared BP-DEX/PEI nanoparticles were examined by TEM and atomic force microscopy (AFM). As shown in Figs. 1 and S1 (online), they are small nanosheets with a size about 15-40 nm and a height of 1.6-4.3 nm (Fig. 1c). The crystal structure of BP-DEX/PEI nanoparticles was determined by powder XRD (Fig. S2a online), and all the peaks in the pattern can be assigned to that of standard orthorhombic black phosphorus (JCPDS No. 76-1957). The chemical composition of BP-DEX/PEI nanoparticles was confirmed by XPS. Figs. 1e, f and S2b (online) show the binding energies of the elements in the sample after calibration with the binding energy of C 1s at 284.6 eV. There are no other elements apart from C, O, N, and P, indicating the high purity of the BP nanoparticles. The N 1s spectrum of BP-DEX/PEI nanoparticles in Fig. 1e shows two peaks at 399.2 and 401.2 eV, which can be attributed to the binding energies of N from C-N and N-H bonds [31], confirming the successful modification of BP with PEI. The two distinct peaks at 129.3 and 130.2 eV are assigned to $2p_{3/2}$ and $2p_{1/2}$ orbitals of zero-valence phosphorous in the P 2p spectrum, respectively (Fig. 1f). The weak peak at 132.7 eV is attributed to oxidized phosphorus (i.e., P⁵⁺) [32], which is due to the partial oxidation of BP nanoparticles during sample preparation and purification.

The surface DEX and PEI, and the partially oxidized surface of functionalized BP nanoparticles endow them with excellent water solubility. Their hydrodynamic size and zeta potential were analyzed by dynamic light scattering (DLS) to be 30.2 nm (Fig. 1d) and 20.0 mV (Fig. 2b), respectively. The negative zeta potential (-41.3 mV) of BP-DEX further supports the partial oxidation of BP nanoparticles and the formation of phosphate groups on the surface. After PEI modification, the zeta potential changed from negative to positive because the PEI possesses abundant amino groups [33]. The hydrodynamic size of BP-DEX/PEI nanoparticles did not change significantly within one week (Fig. S3a online), and the BP-DEX/PEI nanoparticles can be well dispersed in different media, such as H₂O, PBS, low ionic strength saline (NaCl) solution, and 10% fetal bovine serum (FBS) solution (Fig. S3b, c online). The results demonstrate the excellent solubility and colloidal stability of BP-DEX/PEI nanoparticles.

Fig. S4a (online) presents photographs and UV–Vis-NIR absorbance spectra of BP-DEX/PEI nanoparticle solutions with different concentrations. The absorbance of BP-DEX/PEI nanoparticles at 808 nm is linearly increased with BP concentration (Fig. S4b online), which was determined by inductively coupled plasma-optical emission spectroscopy (ICP-OES). According to the Lambert-Beer law ($A/L = \alpha C$, where A is the absorption intensity, L is the length of the cuvette, C is the concentration, and α is the extinction coefficient), the extinction coefficient of the BP-DEX/PEI nanoparticle aqueous solution at 808 nm was calculated to be 1.19 L/(g cm). The small extinction coefficient could be due to the partial oxidation of BP nanoparticles [17].

3.2. Functionalization of BP-DEX/PEI nanoparticles

The surface PEI of BP nanoparticles provides amino groups to conjugate with FA for targeted imaging of tumors. To confirm the successful conjugation, the FTIR spectra of BP-DEX/PEI and BP-DEX/PEI-FA were measured and compared with those of BP. DEX. and BP-DEX, as shown in Figs. 2a and S5 (online). The presence of a small peak at \sim 1,694 cm $^{-1}$ and a small sharp band at \sim 1,598 cm⁻¹ confirm the successful conjugation of FA with these BP-DEX/PEI nanoparticles. The DEX coating on BP is confirmed by the P-O-C peak at \sim 1,000 cm⁻¹ [17] and the PEI coating is proved by the peaks at \sim 1,630 and \sim 1,452 cm⁻¹, which correspond to the N-H vibration and C-N bending vibration [34,35]. Furthermore, the zeta potential of the BP nanoparticles was also measured to confirm their surface modification. After FA modification, the zeta potential is decreased from 20.0 to 7.3 mV (Fig. 2b). The characteristic absorption of pure FA was observed at 280 and 360 nm (Fig. S6 online). Fig. 2c compares the UV-Vis absorption spectra of BP-DEX/ PEI and BP-DEX/PEI-FA nanoparticles. The typical absorption of FA in the spectrum of BP-DEX/PEI-FA nanoparticles is clearly observed, indicating that the FA molecules have been grafted onto BP-DEX/PEI nanoparticles successfully.

In addition, the residual amino groups of BP-DEX/PEI-FA nanoparticles can be used to functionalize with fluorescent dye sulfo-cyanine7 NHS ester (Cy7-SE). After Cy7-SE modification, the zeta potential is further decreased to -24.5 mV (Fig. 2b), and the typical absorption of Cy7 in the absorption spectra of BP-DEX/PEI-FA/Cy7 nanoparticles (Figs. 2c and S7 online) is also observed. An obvious red shift can be found in the spectrum of BP-DEX/PEI-FA/Cy7 nanoparticles, however, in comparison with that of free Cy7, which demonstrates the covalent conjugation of Cy7 with BP-DEX/PEI-FA via the formation of an amide bond. The photoluminescence spectrum of BP-DEX/PEI-FA/Cy7 was recorded under excitation by 750 nm light source, and emission at 780 nm is observed (Fig. 2d).

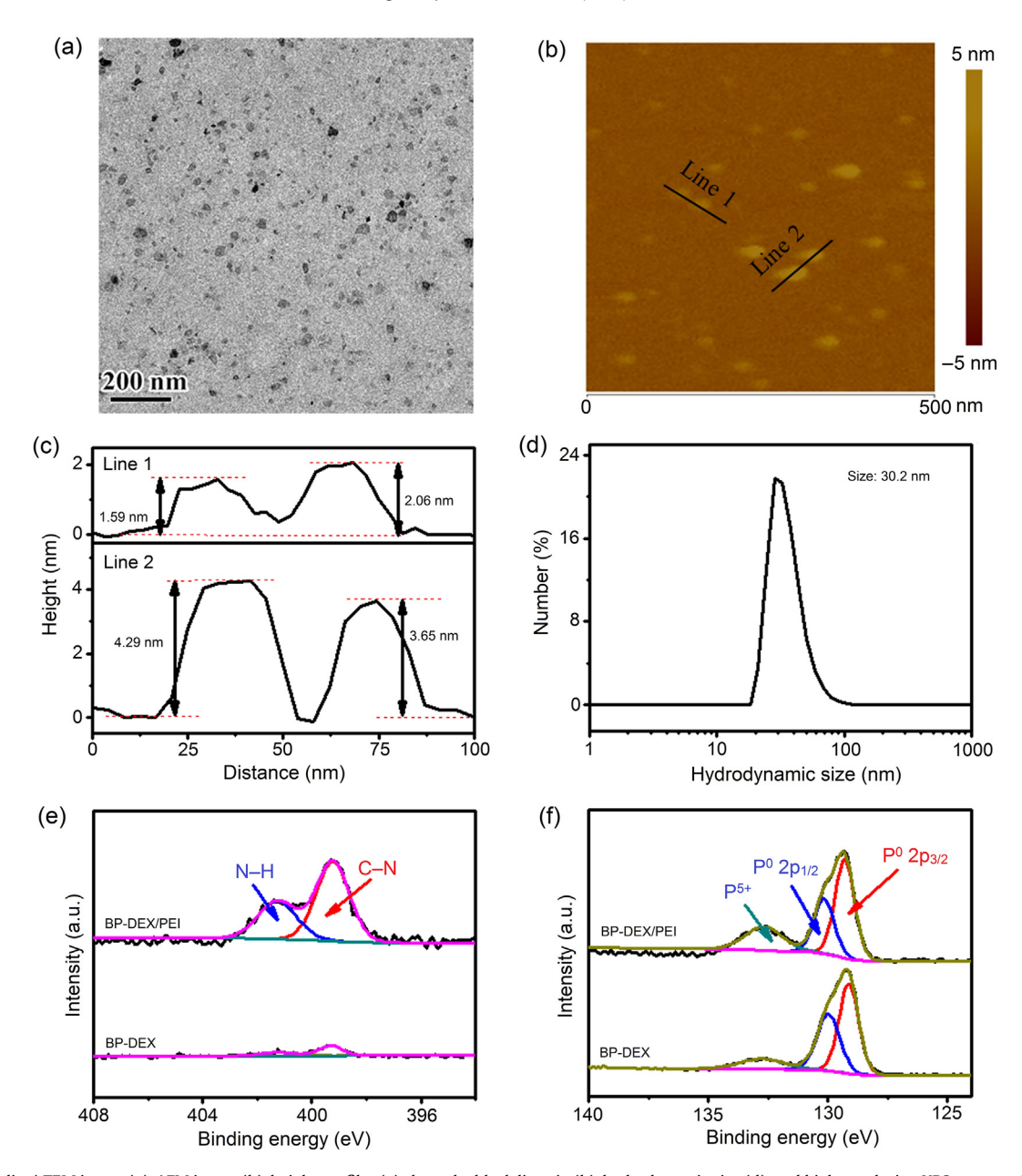


Fig. 1. (Color online) TEM image (a), AFM image (b), height profiles (c) along the black lines in (b), hydrodynamic size (d), and high-resolution XPS spectra of N 1s (e) and P 2p (f) of as-prepared BP-DEX/PEI nanoparticles.

To evaluate the photothermal properties of BP-DEX/PEI-FA/Cv7 nanoparticles, different amounts of nanoparticles were dissolved in aqueous solutions and exposed to an 808 nm NIR laser with a power density of 1.0 W/cm² for 10 min. Fig. 3a clearly demonstrates the concentration-dependent photothermal conversion of BP-DEX/PEI-FA/Cy7 nanoparticles, and the temperature increments (ΔT) can be finely tuned between 5.9 and 32.5 °C by simply changing their concentrations. The photothermal conversion efficiency is calculated to be 41.0%, and the detailed calculations are shown in Fig. S8a, b (online). Furthermore, at the same BP concentration, the temperature increment for the nanoparticles modified with Cy7 is slightly higher (1-4.5 °C) than without Cy7 (Fig. S9a, b online), suggesting that BP-DEX/PEI-FA/Cy7 nanoparticles are more effective in photothermal conversion. To assess the photothermal stability of BP-DEX/PEI-FA/Cy7 nanoparticle solution, the temperature profiles of BP-DEX/PEI-FA/Cy7 were recorded for five successive cycles of heating/cooling processes with an interval of around 30 min (Fig. 3b).

The above remarkable photothermal conversion performance and photothermal stability suggest that the functional BP-DEX/PEI nanoparticles could be a promising photothermal transducer for PA imaging. The in vitro PA imaging was performed with a laser wavelength of 680 nm. The photoacoustic signal is drastically enhanced with the assistance of BP-DEX/PEI-FA nanoparticles, and it is linearly increased with increasing nanoparticle concentration from 0 to 200 $\mu g/mL$ (Fig. 3c). In addition, the potential cytotoxicity of functional BP-DEX/PEI nanoparticles toward healthy cells and cancer cells (3T3, mouse embryo fibroblasts cells, and 4T1, murine breast cancer cells) was investigated by a standard methyl thiazolyl tetrazolium (MTT) assay (Fig. 4a, b). The results demonstrate that the BP-DEX/PEI nanoparticles with or without FA have good biocompatibility, and no serious cytotoxicity toward 4T1 and 3T3 cells was observed in the range of 0–100 $\mu g/mL$.

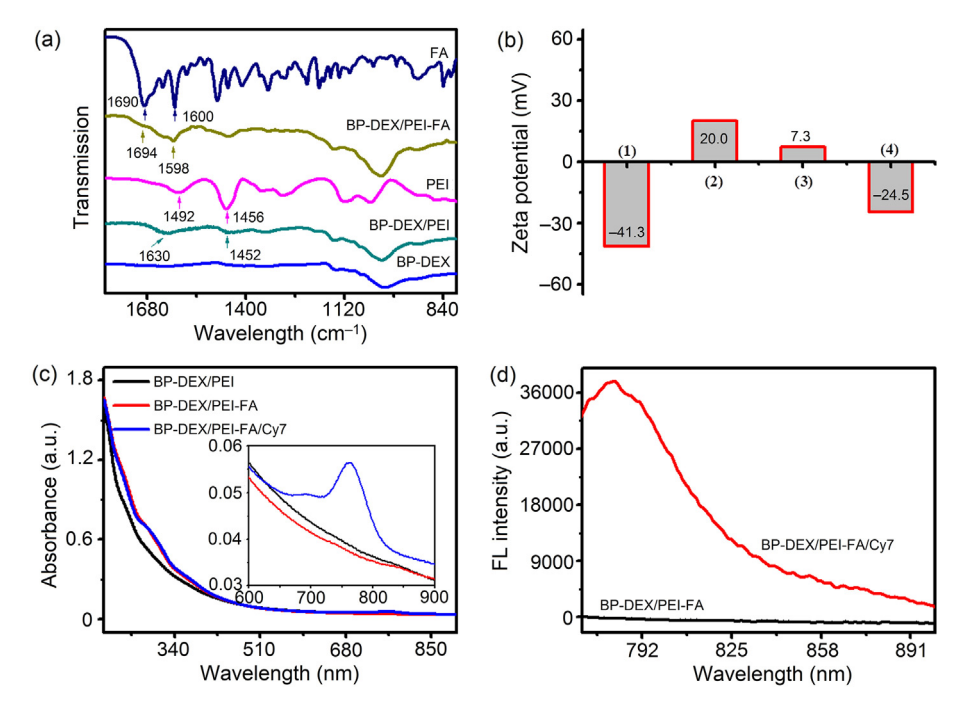


Fig. 2. (Color online) Characterization of as-prepared functionalized BP nanoparticles. (a) FTIR spectra of BP-DEX, BP-DEX/PEI, and BP-DEX/PEI-FA in comparison with those of PEI and FA. (b) The zeta potential of (1) BP-DEX, (2) BP-DEX/PEI, (3) BP-DEX/PEI-FA, and (4) BP-DEX/PEI-FA/Cy7. (c) UV-Vis-NIR spectra of BP-DEX/PEI, BP-DEX/PEI-FA, and BP-DEX/PEI-FA, and BP-DEX/PEI-FA/Cy7, with the inset showing an enlargement of the indicated range. (d) Fluorescence spectra of BP-DEX/PEI-FA and BP-DEX/PEI-FA/Cy7 excited with 750 nm light.

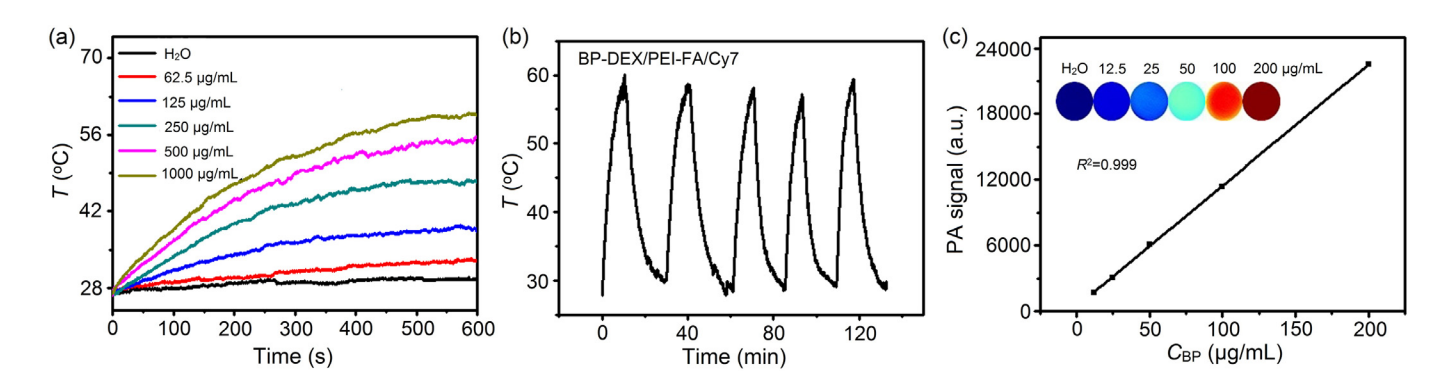


Fig. 3. (Color online) Photothermal and photoacoustic performances of functionalized BP nanoparticles. (a) Photothermal heating curves of pure water and aqueous dispersions of BP-DEX/PEI-FA /Cy7 at different BP concentrations under continuous irradiation by an 808 nm laser with a power density of 1 W/cm² for 10 min. (b) Temperature variation of BP-DEX/PEI-FA/Cy7 nanoparticles solution (1 mg/mL) with five cycles of consecutive laser irradiation (1 W/cm², 10 min) and natural cooling (the time interval between each cycle is about 30 min). (c) Linear fit of photoacoustic intensity to the concentration of BP-DEX/PEI-FA aqueous solution; inset: the corresponding PA images.

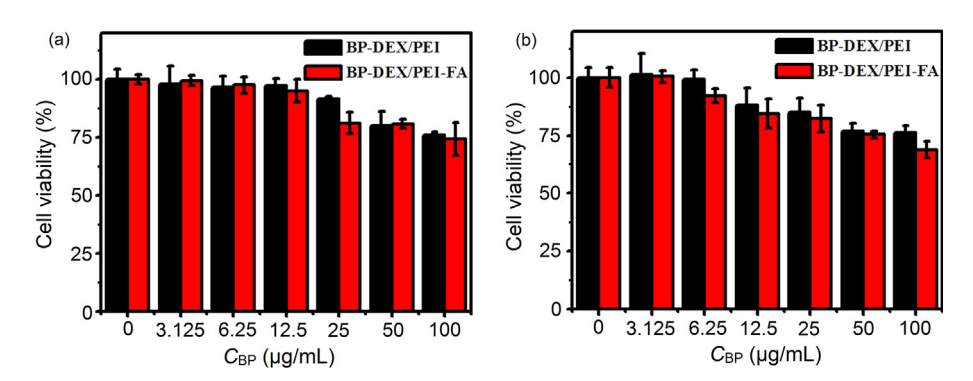


Fig. 4. (Color online) In vitro relative cell viabilities of 4T1 (a) and 3T3 (b) cells determined by MTT assay, after they were cultured with different concentrations (0, 3.125, 6.25, 12.5, 25, 50, and 100 μ g/mL) of BP-DEX/PEI and BP-DEX/PEI-FA nanoparticles for 12 h, respectively.

3.3. In vivo imaging

As mentioned previously, BP-DEX/PEI-FA nanoparticles show great potential in targeted PA imaging. Therefore, BP-DEX/PEI nanoparticles with or without FA were intravenously injected into 4T1 tumor-bearing nude mice, and then a set of PA images of the tumor region was acquired before and after injection. Figs. 5a and S10 (online) present the PA images and the signals from the tumor site obtained at different times. These results indicate that the signal is gradually increased with the circulation of nanoparticles after their intravenous injection. The PA signals reached their maximum intensity at 8 h post injection and then decreased. The maximum signals obtained from BP-DEX/PEI and BP-DEX/PEI-FA nanoparticles are 2.4 and 3.1 times higher than that of the precontrast image, respectively. The stronger signal from BP-DEX/PEI-FA nanoparticles is attributed to the targeting capability of FA and the enhanced permeability and retention (EPR) effect.

To further demonstrate the in vivo targeting effect of BP-DEX/PEI-FA nanoparticles, the same amounts of BP-DEX/PEI-Cy7 and BP-DEX/PEI-FA/Cy7 were intravenously injected into mice bearing 4T1 tumors, and NIRF images were acquired at different time points. As shown in Fig. 5b, strong fluorescence signals were observed in the whole mouse at the beginning (15 min post injection) in both cases. Then, the fluorescence signals gradually decreased, and the signal from BP-DEX/PEI-FA/Cy7 nanoparticles was higher than that from BP-DEX/PEI-Cy7 nanoparticles, due to the conjugation of FA with nanoparticles to enhance their stability and accumulation in the tumor. These results could further verify the in vivo targeting effect of BP-DEX/PEI-FA nanoparticles.

3.4. In vivo photothermal therapy

As mentioned previously, BP-DEX/PEI-FA/Cy7 nanoparticles show potential in photothermal therapy. Although the accumulated BP nanoparticles are sufficient for imaging to diagnose the

tumor after they were intravenously injected ($200 \,\mu\text{L}$, $2 \,\text{mg/mL}$), they could not produce enough heat for photothermal therapy if the same amount of nanoparticles is intravenously injected. Therefore, BP nanoparticles were intratumorally injected, and only one quarter ($50 \,\mu\text{L}$, $2 \,\text{mg/mL}$) of dosage used for imaging is enough to kill cancer cells by photothermal therapy. Four groups of 4T1 tumor-bearing BALB/c mice ($5 \,\text{mice/group}$) were respectively intratumorally injected with BP-DEX/PEI-FA/Cy7 nanoparticles ($2 \,\text{mg/mL}$, $50 \,\mu\text{L}$) or PBS solution ($50 \,\mu\text{L}$). The mice in the treatment group were then irradiated for $6 \,\text{min}$ by an 808 nm NIR laser with a power density of $1.5 \,\text{W/cm}^2$. Three other control groups are referred to as (1) mice without any treatment (control group), (2) mice only injected with BP-DEX/PEI-FA/Cy7 nanoparticles without laser irradiation (BP-DEX/PEI-FA/Cy7 group), and (3) mice injected with PBS and irradiated with the laser (PBS + NIR group).

During the NIR laser irradiation, the tumor temperature of the mice was monitored by an infrared thermal camera. As shown in Fig. 6a, b, the tumor temperature of mice in the treatment group increased quickly and reached 64 °C within 6 min, higher than that of PEGylated BP nanoparticles [17], which may be due to the fact that FA facilitates the uptake of BP-DEX/PEI-FA/Cy7 nanoparticles by tumor cells. The tumor temperature of the treatment group is much higher than that of the mice injected with PBS (44 °C), which is enough for ablating the cancer cells.

The tumor volume (Fig. 6c), the body weights (Fig. 6d), and photographs (Fig. S11 online) of the mice were measured and taken every 2 d after the treatments. The weights of four groups of mice showed negligible differences, which indicates that the current dose of BP-DEX/PEI-FA/Cy7 nanoparticles did not induce acute toxicity. The tumors of mice injected with the BP-DEX/PEI-FA/Cy7 nanoparticles followed by laser irradiation gradually shrank and were completely cured within 15 d. No recurrence was observed in this treatment group until the mice were sacrificed after 30 d (Fig. S12 online). To further determine that the therapeutic efficacy of BP-DEX/PEI-FA/Cy7 nanoparticles, the major organs of mice

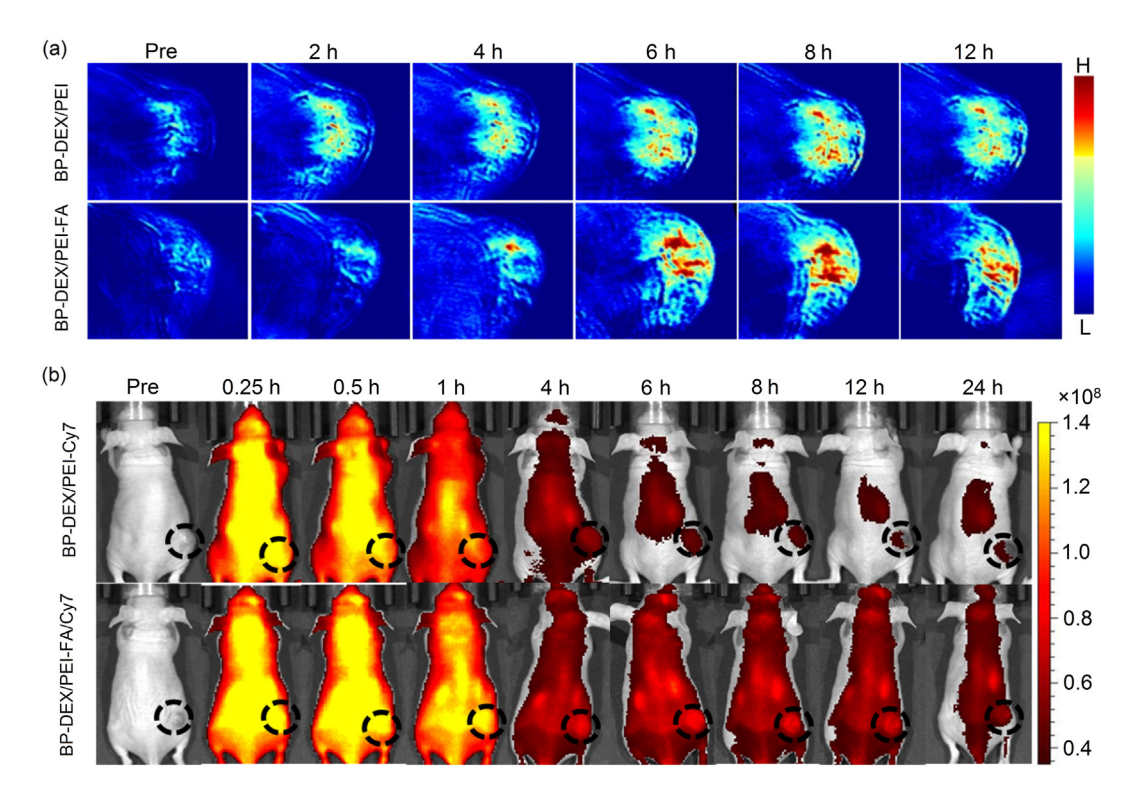


Fig. 5. (Color online) Targeted imaging of tumor with BP-DEX/PEI-FA nanoparticles. (a) In vivo PA images of the 4T1 tumor-bearing mice before and after tail vein injection of BP-DEX/PEI and BP-DEX/PEI-FA nanoparticles (200 μ L, 2 mg/mL) at different time points. (b) In vivo NIRF images of the 4T1 tumor-bearing mice before and after tail vein injection of BP-DEX/PEI-Cy7 and BP-DEX/PEI-FA/Cy7.

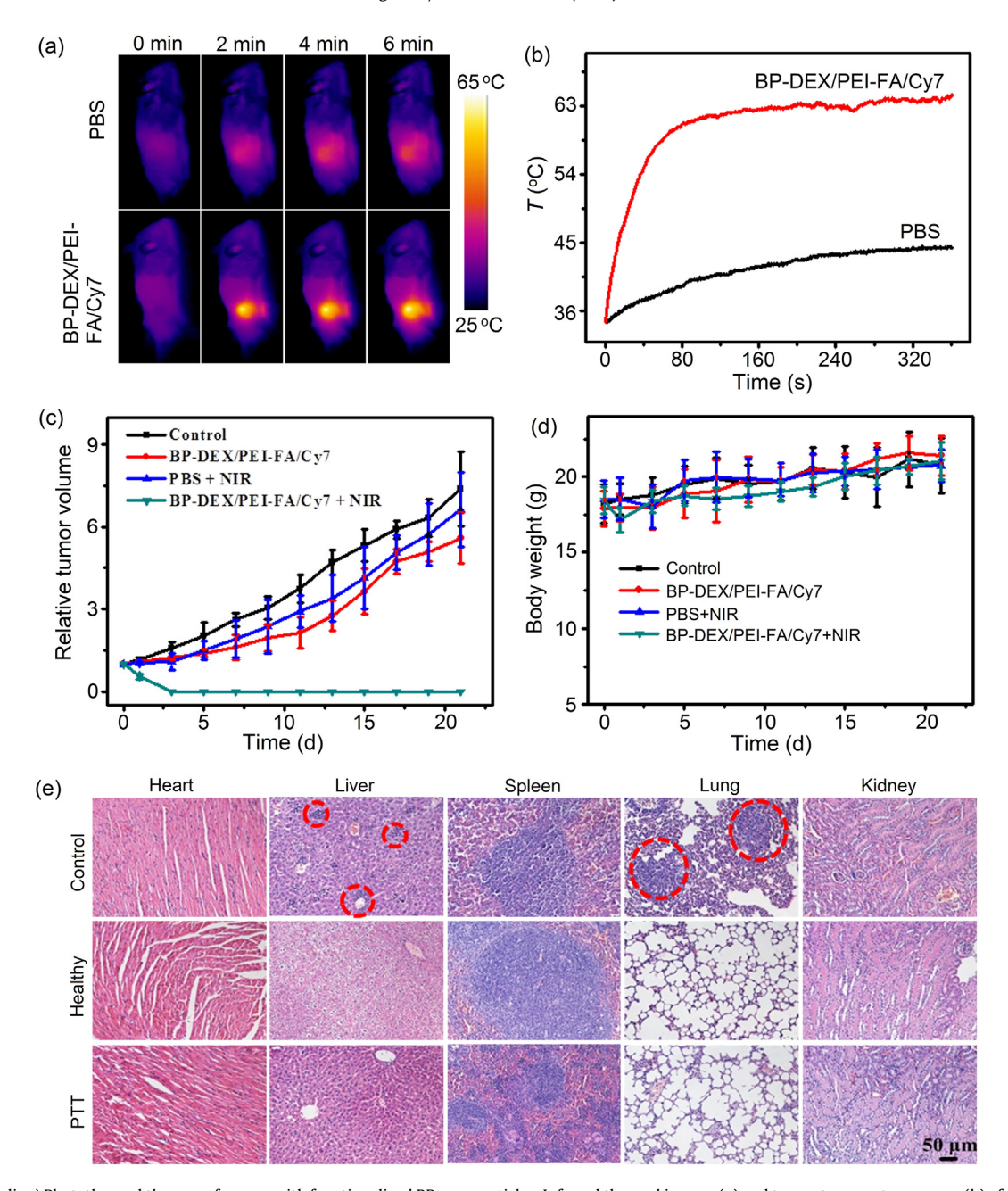


Fig. 6. (Color online) Photothermal therapy of cancer with functionalized BP nanoparticles. Infrared thermal images (a) and tumor temperature curves (b) of mice bearing 4T1 tumors after injection of BP-DEX/PEI-FA/Cy7 solution or PBS and then irradiation with an 808 nm NIR laser at a power density of 1.5 W/cm² for 6 min. The relative tumor volumes normalized to the original volumes (c) and the average body weights (d) of mice after the treatments. (e) H&E stained images of major organs from the healthy mice, the control group, and treatment group (with the organs collected after 30 d of therapy).

were harvested at day 30 after treatment, which were sliced and stained with H&E. As shown in Fig. 6e, there were obvious metastases in the livers and lungs of mice in the control group compared with healthy mice. In contrast, no metastasis was observed in organs of the mice treated by photothermal therapy with BP-DEX/PEI-FA/Cy7 nanoparticles, which further confirms the effectiveness and safety of BP-DEX/PEI-FA/Cy7 nanoparticles for PTT.

4. Conclusions

In summary, 20-nm BP-DEX/PEI nanoparticles were prepared by a solventless one-pot high energy mechanical milling (HEMM) approach and subsequently functionalized with FA and Cy7 by

covalent conjugation. The resultant BP-DEX/PEI-FA/Cy7 small nanoparticles exhibit excellent water-solubility, colloidal stability, biocompatibility, and high photothermal conversion efficiency for in vivo targeted imaging (PA, NIRF) and photothermal therapy of cancer. The tumor images obtained from BP nanoparticles conjugated with FA exhibit better brightness and higher intensity than those from BP nanoparticles without FA. The therapy results also show excellent performance of BP-DEX/PEI-FA/Cy7 nanoparticles. These multifunctional BP nanoparticles hold promise for the diagnosis and treatment of cancer.

Conflict of interest

The authors declare that they have no conflict of interest.

Acknowledgments

Zhen Li acknowledges support from the National Natural Science Foundation of China (81471657, 81527901), the 1000 Plan for Young Talents, Jiangsu Specially Appointed Professorship, and Jiangsu Provincial Program for Innovative and Entrepreneurial Talents. The authors also are grateful for support from the Jiangsu Provincial Key Laboratory of Radiation Medicine and Protection, the Priority Academic Development Program of Jiangsu Higher Education Institutions (PAPD). The authors would like to thank Dr. Tania Silver for critical reading of the manuscript.

Appendix A. Supplementary data

Supplementary data associated with this article can be found, in the online version, at https://doi.org/10.1016/j.scib.2018.05.022.

References

- [1] Huo C, Yan Z, Song X, et al. 2D materials via liquid exfoliation: a review on fabrication and applications. Sci Bull 2015;60:1994–2008.
- [2] Dong Y, Wu ZS, Ren W, et al. Graphene: a promising 2D material for electrochemical energy storage. Sci Bull 2017;62:724–40.
- [3] Bridgman PW. Two new modifications of phosphorus. J Am Chem Soc 1914;36:1344-63.
- [4] Sun J, Zheng G, Lee HW, et al. Formation of stable phosphorus-carbon bond for enhanced performance in black phosphorus nanoparticle-graphite composite battery anodes. Nano Lett 2014;14:4573–80.
- [5] Xia F, Wang H, Jia Y. Rediscovering black phosphorus as an anisotropic layered material for optoelectronics and electronics. Nat Commun 2014;5:4458.
- [6] Tran V, Soklaski R, Liang Y, et al. Layer-controlled band gap and anisotropic excitons in few-layer black phosphorus. Phys Rev B 2014;89:235319.
- [7] Wang H, Wang X, Xia F, et al. Black phosphorus radio-frequency transistors. Nano Lett 2014;14:6424–9.
- [8] Du H, Lin X, Xu Z, et al. Recent developments in black phosphorus transistors. J Mater Chem C 2015;3:8760–75.
- [9] Feng Q, Yan F, Luo W, et al. Charge trap memory based on few-layer black phosphorus. Nanoscale 2016:8:2686–92.
- [10] Engel M, Steiner M, Avouris P. Black phosphorus photodetector for multispectral, high-resolution imaging, Nano Lett 2014;14:6414–7.
- [11] Erande MB, Pawar MS, Late DJ. Humidity sensing and photodetection behavior of electrochemically exfoliated atomically thin-layered black phosphorus nanosheets. ACS Appl Mater Interfaces 2016;8:11548–56.
- [12] Li W, Yang Y, Zhang G, et al. Ultrafast and directional diffusion of lithium in phosphorene for high-performance lithium-ion battery. Nano Lett 2015:15:1691–7.
- [13] Yao Q, Huang C, Yuan Y, et al. Theoretical prediction of phosphorene and nanoribbons as fast-charging Li ion battery anode materials. J Phys Chem C 2015;119:6923–8.
- [14] Kou L, Frauenheim T, Chen C. Phosphorene as a superior gas sensor: selective adsorption and distinct *I-V* response. J Phys Chem Lett 2014;5:2675–81.
- [15] Cho S, Lee Y, Koh H, et al. Superior chemical sensing performance of black phosphorus: comparison with MoS₂ and graphene. Adv Mater 2016:28:7020–8
- [16] Lee HU, Park SY, Lee SC, et al. Black phosphorus (BP) nanodots for potential biomedical applications. Small 2016;12:214–9.
- [17] Sun C, Wen L, Zeng J, et al. One-pot solventless preparation of PEGylated black phosphorus nanoparticles for photoacoustic imaging and photothermal therapy of cancer. Biomaterials 2016;91:81–9.
- [18] Sun Z, Zhao Y, Li Z, et al. TiL₄-coordinated black phosphorus quantum dots as an efficient contrast agent for in vivo photoacoustic imaging of cancer. Small 2017;13:1602896.
- [19] Sun Z, Xie H, Tang S, et al. Ultrasmall black phosphorus quantum dots: synthesis and use as photothermal agents. Angew Chem Int Ed 2015;54:11526–30.
- [20] Wang H, Yang X, Shao W, et al. Ultrathin black phosphorus nanosheets for efficient singlet oxygen generation. J Am Chem Soc 2015;137:11376–82.
- [21] Tao W, Zhu X, Yu X, et al. Black phosphorus nanosheets as a robust delivery platform for cancer theranostics. Adv Mater 2017;29:1603276.
- [22] Yang D, Yang G, Yang P, et al. Assembly of Au plasmonic photothermal agent and iron oxide nanoparticles on ultrathin black phosphorus for targeted photothermal and photodynamic cancer therapy. Adv Funct Mater 2017;27:1700371.
- [23] Almeida J, Chen A, Foster A, et al. In vivo biodistribution of nanoparticles. Nanomedicine 2011;6:815–35.
- [24] Liu C, Gao Z, Zeng J, et al. Magnetic/upconversion fluorescent NaGdF₄:Yb, Er nanoparticle-based dual-modal molecular probes for imaging tiny tumors in vivo. ACS Nano 2013;7:7227–40.

- [25] Wang Y, Yang T, Ke H, et al. Smart albumin-biomineralized nanocomposites for multimodal imaging and photothermal tumor ablation. Adv Mater 2015;27:3874–82.
- [26] Jiang X, Zhang S, Ren F, et al. Ultrasmall magnetic CuFeSe₂ ternary nanocrystals for multimodal imaging guided photothermal therapy of cancer. ACS Nano 2017;11:5633–45.
- [27] Mao F, Wen L, Sun C, et al. Ultrasmall biocompatible Bi₂Se₃ nanodots for multimodal imaging-guided synergistic radiophotothermal therapy against cancer. ACS Nano 2016;10:11145–55.
- [28] Wen L, Chen L, Zheng S, et al. Ultrasmall biocompatible WO_{3-x} nanodots for multi-modality imaging and combined therapy of cancers. Adv Mater 2016;28:1506428.
- [29] Zhang S, Huang Q, Zhang L, et al. Vacancy engineering of Cu_{2-x}Se nanoparticles with tunable lspr and magnetism for dual-modal imaging guided photothermal therapy of cancer. Nanoscale 2018;10:3130–43.
- [30] Zhang S, Sun C, Zeng J, et al. Ambient aqueous synthesis of ultrasmall pegylated Cu_{2-x}Se nanoparticles as a multifunctional theranostic agent for multimodal imaging guided photothermal therapy of cancer. Adv Mater 2016;28:8927–36.
- [31] Zhang M, Zhao X, Fang Z, et al. Fabrication of HA/PEI-functionalized carbon dots for tumor targeting, intracellular imaging and gene delivery. RSC Adv 2017;7:3369–75.
- [32] Kang J, Wood JD, Wells SA, et al. Solvent exfoliation of electronic-grade, twodimensional black phosphorus. ACS Nano 2015;9:3596-604.
- [33] Wang L, Meng D, Hao Y, et al. A gold nanostar based multi-functional tumortargeting nanoplatform for tumor theranostic applications. J Mater Chem B 2016;4:5895–906.
- [34] Shi J, Liu Y, Wang L, et al. A tumoral acidic pH-responsive drug delivery system based on a novel photosensitizer (fullerene) for in vitro and in vivo chemophotodynamic therapy. Acta Biomater 2014;10:1280–91.
- [35] Wang J, Zhang B, Wang L, et al. One-pot synthesis of water-soluble superparamagnetic iron oxide nanoparticles and their MRI contrast effects in the mouse brains. Mater Sci Eng C 2015;48:416–23.



Lijuan Deng received bachelor of engineering degree in 2015 from Guangxi University of China. She is the Master Candidate of Material Science and Engineering, East China University of Science and Technology. She is doing Master on functionalization of black phosphorus for biomedical applications, under supervision of Prof. Zhen Li in the Center for Molecular Imaging and Nuclear Medicine at Soochow University.



Chongjun Zhao received his Ph.D. in physical chemistry in 2002 from Fudan University of China. He has been an associate professor of material science and technology in East China University of Science and Technology since 2006. His research interests are tunable synthesis of interioral transition metal oxides (sulfides) and their applications in various fields including electrochemical biosensor, energy storage (supercapacitor, Li-ion battery), photocatalysis.



Zhen Li received his Ph.D. degree from the Institute of Chemistry, Chinese Academy of Sciences in 2005, and then successively worked in the University of Liverpool, University of Siegen, University of Queensland and University of Wollongong for 9 years. He joined the School of Radiation Medicine and Protection, Soochow University in 2014. His research focuses on multifunctional nanomaterials for biomedical and energy applications.